2013 IEEE/RSJ International Conference on
Intelligent Robots and Systems (IROS)
November 3-7, 2013. Tokyo, Japan

A Robust Visual Servo Control Scheme with Prescribed Performance for an Autonomous Underwater Vehicle

Charalampos P. Bechlioulis[1], George C. Karras[1], Sharad Nagappa[2], Narcís Palomeras[2], Kostas J. Kyriakopoulos[1], Marc Carreras[2]

Abstract— **This paper describes the design and implementation of a visual servo control scheme for an Autonomous Underwater Vehicle (AUV). The purpose of the control scheme is to navigate and stabilize the vehicle towards a visual target. The controller does not utilize the vehicle's dynamic model parameters and guarantees prescribed transient and steady state performance despite the presence of external disturbances representing ocean currents and waves. The proposed control scheme is of low complexity and can be easily integrated to an embedded control platform of an Autonomous Underwater Vehicle (AUV) with limited power and computational resources. Moreover, through the appropriate selection of certain performance functions, the proposed scheme guarantees that the target lies inside the onboard camera's field of view for all time. The resulting control scheme has analytically guaranteed stability and convergence properties, while its applicability and performance are experimentally verified using the Girona500 AUV.**

I. INTRODUCTION

Underwater vehicles usually operate under difficult circumstances and perform complex tasks such as ship hull inspection, surveillance of underwater facilities (e.g oil platforms) and handling of underwater equipment (e.g control panels, valves) etc. These tasks require motion control schemes with enhanced robustness and a sensor suite that can provide an accurate and detailed description of the underwater environment. When an underwater vehicle operates autonomously, the use of onboard cameras is of utmost importance. Monocular or stereo vision systems can provide information regarding target tracking or pose estimation that can be incorporated to the motion or force control schemes of the vehicle, depending on the task and the mission properties.

Concerning visual servo control in underwater robotics, an application of image based visual servoing was realized in [1]. In that case the vehicle was fully actuated, implying that the camera had 6 degrees of freedom (DOF). Interesting stereo vision approaches can be found at [2], [3]. The problem of keeping the target inside the field of view has been examined in the past, in robotic manipulators [4], cartesian robots [5], differential drive mobile robots [6], [7] and underwater vehicles [8]. The proposed methodologies were based on complex path planning techniques while the computed points were fed to kinematic controllers designed for point to point motions or stabilization at a fixed point in the workspace. Also, a model-based switching visual servo control scheme for the semi-autonomous operation of an under-actuated Remotely Operated Vehicle (ROV) has been presented in [9]. In all the above schemes, the controller was either model-based (i.e., an accurate dynamic model of the vehicle is required) or strictly kinematic, without guaranteed performance in the presence of external disturbances such as ocean currents and waves.

In this paper, a novel position–based visual servo control scheme for an Autonomous Underwater Vehicle is presented. The controller is responsible for navigating and stabilizing the AUV in front of a panel consisting of various valves and handles. It does not utilize the vehicle's dynamic model parameters and guarantees prescribed transient and steady state performance despite the presence of external disturbances. Moreover, through the appropriate selection of certain performance functions, the proposed scheme guarantees also the satisfaction of visual constraints which in this case are defined as keeping the target inside the camera's field of view. A high level computer vision algorithm tracks the panel and calculates its pose vector with respect to the vehicle. The pose vector is fused with the rest of the navigation measurements using an extended Kalman filter (EKF). The resulting estimated state vector is used as state feedback to the proposed motion control scheme. The applicability and performance of the overall system are demonstrated using the Girona500 AUV in a test pool, where a valve panel is appropriately mounted.

II. PRELIMINARIES

A. AUV Kinematics and Dynamics

The visual servo control scheme proposed in this work is applied to the Girona500 AUV. A simplified 3D dynamic model (in surge, sway, heave and yaw) of the vehicle is presented in this subsection in accordance to the standard underwater vehicle modeling properties [10]. The roll and pitch degrees of freedom are neglected for the clarity of the presentation and owing to page limitations. It will be mentioned in the sequel, however, that both degrees of freedom can be considered in the analysis without compromising the achieved results. In this respect, consider the vehicle modeled as a rigid body subject to external forces and torques. Let $\{I\}$ be an inertial coordinate frame and $\{B\}$ a body-fixed coordinate frame, whose origin O_B is located at the center of

This work was supported by the EU funded project PANDORA: Persistent Autonomy through learNing, aDaptation, Observation and ReplAnning", FP7-288273, 2012-2014.

[1]School of Mechanical Engineering, National Technical University of Athens, Athens 15780, Greece {chmpechl, karrasg, kkyria}@mail.ntua.gr.

[2]University of Girona, Edifici Politecnica IV, Campus Montilivi, Girona 17071, Spain {snagappa, npalomer, marcc}@eia.udg.edu.

978-1-4673-6357-0/13/$31.00 ©2013 IEEE

mass of the vehicle. Furthermore, let (x,y,z) be the position of O_B in $\{I\}$ and ψ denote the yaw angle. Let (u,v,w) be the longitudinal (surge), transverse (sway) and vertical (heave) velocities of O_B with respect to $\{I\}$ expressed in $\{B\}$ and r be the vehicle's angular speed (yaw) around the vertical axis. Thus, the kinematic equations of motion for the considered vehicle can be written as:

$$\dot{x} = u\cos\psi - v\sin\psi + \delta_x(t) \tag{1}$$
$$\dot{y} = u\sin\psi + v\cos\psi + \delta_y(t) \tag{2}$$
$$\dot{z} = w + \delta_z(t) \tag{3}$$
$$\dot{\psi} = r + \delta_\psi(t) \tag{4}$$

where $\delta_x(t)$, $\delta_y(t)$, $\delta_z(t)$, $\delta_\psi(t)$ denote bounded ocean currents. Neglecting the motion in roll and pitch, the simplified equations for the surge, sway, heave and yaw can be written as:

$$m_u\dot{u} = m_v vr + X_u u + X_{|u|u}|u|u + X + \delta_u(t) \tag{5}$$
$$m_v\dot{v} = -m_u ur + Y_v v + Y_{|v|v}|v|v + Y + \delta_v(t) \tag{6}$$
$$m_w\dot{w} = Z_w w + Z_{|w|w}|w|w + (W-B) + Z + \delta_w(t) \tag{7}$$
$$m_r\dot{r} = (m_u - m_v)uv + N_r r + N_{|r|r}|r|r + N + \delta_r(t) \tag{8}$$

where m_u, m_v, m_w, m_r denote the vehicle's mass, moment of inertia, added mass and moment of inertia terms, X_u, $X_{|u|u}$, Y_v, $Y_{|v|v}$, Z_w, $Z_{|w|w}$, N_r, $N_{|r|r}$ are negative hydrodynamic damping coefficients of first and second order, W and B are the vehicle weight and buoyancy respectively, $\delta_u(t)$, $\delta_v(t)$, $\delta_w(t)$, $\delta_r(t)$ denote bounded exogenous forces and torques acting on surge, sway, heave and around yaw owing to ocean waves and X, Y, Z, N denote the control input forces and torque respectively that are applied by the thrusters in order to produce the desired motion of the body fixed frame.

B. Navigation Module

The navigation module is responsible for estimating the vehicle position and velocity vector. The linear positions ($[x\ \ y\ \ z]$) and velocities ($[u\ \ v\ \ w]$) are estimated using a Vision EKF SLAM algorithm, while the angular positions ($[\phi\ \ \theta\ \ \psi]$) and velocities ($[p\ \ q\ \ r]$) are directly measured using an internal motion reference unit (IMU). The Vision EKF SLAM algorithm provides simultaneously estimation updates for the visual landmarks and the linear positions and velocities of the vehicle.

The augmented system model (vehicle and landmarks) consists of a constant velocity kinematic model for the vehicle and a constant time model for the landmarks. Regarding the measurement models, position and velocity sensors are available. A global positioning system (GPS) measures the vehicle position in $(x,\ y)$ plane when the vehicle is not submerged and a pressure sensor transforms pressure values into depth measurements (z). The velocity updates are provided by a doppler velocity log (DVL). This sensor is able to measure linear velocities with respect to the sea bottom or the water around the vehicle. The pose and velocity updates are direct measurements of the state vector.

If only these two updates are available, the navigation module is a dead reckoning algorithm that drifts over time. However, if landmarks are detected in the environment, the navigation module is able to keep its position covariance bounded. A visual detection algorithm, detailed in section III-A, gives information about the relative position of a landmark with respect to the vehicle. This information not only updates the detected landmark position but also the vehicle. The visual detection algorithm uses an *a priori* known template to identify and compute the relative position of these landmarks.

The mathematical description of the navigation module and the Visual EKF SLAM algorithm are trivial and thus omitted.

C. Prescribed Performance

It will be clearly demonstrated in Subsection III-B, that the control design is connected to the prescribed performance notion that was originally employed to design neuro-adaptive controllers for various classes of nonlinear systems [11]–[13], capable of guaranteeing output tracking with prescribed performance. In this work, by prescribed performance, it is meant that the tracking error converges to a predefined arbitrarily small residual set with convergence rate no less than a certain predefined value. For completeness and compactness of presentation, this subsection summarizes preliminary knowledge on prescribed performance. Thus, consider a generic scalar error $e(t)$. Prescribed performance is achieved if $e(t)$ evolves strictly within a predefined region that is bounded by decaying functions of time. The mathematical expression of prescribed performance is given, $\forall t \geq 0$, by the following inequalities:

$$-\rho(t) < e(t) < \rho(t) \tag{9}$$

where $\rho(t)$ is a smooth, bounded, strictly positive and decreasing function of time satisfying $\lim_{t\to\infty}\rho(t) > 0$, called performance function [11]. Hence, for an exponentially decreasing performance function $\rho(t) = (\rho_0 - \rho_\infty)e^{-lt} + \rho_\infty$ with ρ_0, ρ_∞, l, the constant $\rho_0 = \rho(0)$ is selected such that $\rho_0 > |e(0)|$, the constant $\rho_\infty = \lim_{t\to\infty}\rho(t)$ represents the maximum allowable size of the tracking error $e(t)$ at the steady state and finally the decreasing rate of $\rho(t)$, which is affected by the constant l in this case, introduces a lower bound on the required speed of convergence of $e(t)$.

D. Dynamical Systems

Consider the initial value problem:

$$\dot{\xi} = h(t,\xi),\ \xi(0) = \xi^0 \in \Omega_\xi \tag{10}$$

with $h : \Re_+ \times \Omega_\xi \to \Re^n$ where $\Omega_\xi \subset \Re^n$ is a non-empty open set.

Definition 1: [14] A solution $\xi(t)$ of the initial value problem (10) is maximal if it has no proper right extension that is also a solution of (10).

Theorem 1: [14] Consider the initial value problem (10). Assume that $h(t,\xi)$ is: a) locally Lipschitz on ξ for almost all $t \in \Re_+$, b) piecewise continuous on t for each fixed $\xi \in \Omega_\xi$ and c) locally integrable on t for each fixed $\xi \in \Omega_\xi$.

Then, there exists a maximal solution $\xi(t)$ of (10) on the time interval $[0,\ \tau_{\max})$ with $\tau_{\max} > 0$ such that $\xi(t) \in \Omega_\xi$, $\forall t \in [0,\ \tau_{\max})$.

Proposition 1: [14] Assume that the hypotheses of Theorem 1 hold. For a maximal solution $\xi(t)$ on the time interval $[0,\ \tau_{\max})$ with $\tau_{\max} < \infty$ and for any compact set $\Omega'_\xi \subset \Omega_\xi$ there exists a time instant $t' \in [0,\ \tau_{\max})$ such that $\xi(t') \notin \Omega'_\xi$.

III. METHODOLOGY

A. Valve Panel Tracking

Position control relies on the use of position measurements with respect to a static external reference. In this work, the vehicle is required to hover in front of an underwater panel for an intervention task; in this respect, the panel provides an external reference if we are able to accurately measure its distance from the vehicle. Detection of the underwater panel is performed using vision, by comparing the images from the camera against an *a priori* known template of the panel. By detecting and matching features between the camera image and template, it is possible to detect the presence of the panel, as well as accurately estimate the pose when a sufficient number of features are matched.

In this work, we choose the oriented FAST and rotated BRIEF (ORB) [15] feature extractor for its suitability to real-time applications. The ORB feature extractor relies on features from accelerated segment test (FAST) corner detection [16] to detect keypoints in the image. These are obvious features to detect on man-made structures and can be detected very quickly. Moreover, there is a (binary) descriptor vector of the keypoint based on binary robust independent elementary features (BRIEF) [17]. Differences between descriptors can be calculated rapidly, allowing real-time matching of keypoints at higher image frame-rates when compared to other commonly used feature extractors such as scale invariant feature transform (SIFT) [18] and speeded-up robust features (SURF) [19].

A minimum number of keypoints must be matched between the template and the camera image to satisfy the panel detection requirement. A low number of matched keypoints indicates that the panel is not in the camera field of view. The correspondences between the template and camera image can be used to compute the transformation (or homography) of the template image to the detected panel in the camera image. This allows us to compute the image-coordinates of the corners of the panel in the camera image. Then, using the known geometry of the panel and the camera matrix, we are able to determine the pose of the panel in the camera coordinate system. Once the panel is detected as a landmark, it can be added to the list of landmarks as discussed previously, and subsequent updates to the panel pose are incorporated through the EKF-SLAM algorithm.

B. Visual Servo Control Scheme with Prescribed Performance

Let x_d, y_d, z_d denote the position of the center of the target and $n_d = \left[n_{x_d}, n_{y_d}, n_{z_d}\right]^T$ denotes the normal to the target plane vector pointing inwards, obtained both via the aforementioned visual tracking system. The objective of this paper is to design a controller without incorporating any information regarding the vehicle model such that it hovers in front of the target with bounded closed loop signals and prescribed transient and steady state performance despite the presence of exogenous disturbances representing ocean currents and waves. Moreover, assuming that the target initially lies inside the onboard camera's field of view, the controller should guarantee that the target never escapes it. Such configuration constraint is important in visual servo control schemes where the feedback depends mainly on the visual contact of the vehicle and the target.

Let us now define the position errors:

$$e_x = x - (x_d - \bar{d}n_{x_d}), e_y = y - (y_d - \bar{d}n_{y_d}), e_z = z - (z_d - \bar{d}n_{z_d}), \tag{11}$$

with $\bar{d}$ denoting the desired distance from the center of the target, where the vehicle should hover. Let us also define the desired yaw angle $\psi_d(x,y)$ as follows:

$$\psi_d(x,y) = \tan^{-1}\left(\frac{y_d - y}{x_d - x}\right) \tag{12}$$

and the orientation error:

$$e_\psi = \psi - \psi_d(x,y). \tag{13}$$

It can be easily verified that the desired orientation $\psi_d(x,y)$, which depends on the current position of the vehicle on the horizontal plane (x,y), is the angle that the vector $[x_d - x,\ y_d - y]^T$ (i.e., the vector defined from the vehicle to the target) forms from the x-axis of the inertial frame. We have designed the desired yaw angle as in (12) because we want to incorporate in our analysis the orientation constraint owing to the limited field of view of the onboard camera. Notice forcing the orientation error (13) close to zero satisfying simultaneously $\left|e_\psi(t)\right| < \psi_c$, $\forall t \geq 0$, where ψ_c denotes the camera's angle of view, moving towards the target (i.e., forcing position errors (11) to zero) achieves both control objectives, i.e., hovering in front of the target and keeping the target in the camera's field of view.

1) Control Scheme: Given the position of the center of the target x_d, y_d, z_d, the normal to the target plane vector $n_d = \left[n_{x_d}, n_{y_d}, n_{z_d}\right]^T$ pointing inwards and the position/orientation errors (11)-(13):

I. Kinematic Controller

Select the exponentially decaying position/orientation performance functions $\rho_x(t)$, $\rho_y(t)$, $\rho_z(t)$, $\rho_\psi(t)$ that i) satisfy:

a. $\lvert e_x(0)\rvert < \rho_x(0)$	$0 < \rho_x(t)$	$0 < \lim_{t\to\infty} \rho_x(t)$
b. $\lvert e_y(0)\rvert < \rho_y(0)$	$0 < \rho_y(t)$	$0 < \lim_{t\to\infty} \rho_y(t)$
c. $\lvert e_z(0)\rvert < \rho_z(0)$	$0 < \rho_z(t)$	$0 < \lim_{t\to\infty} \rho_z(t)$
d. $\lvert e_\psi(0)\rvert < \rho_\psi(0) < \psi_c$	$0 < \rho_\psi(t)$	$0 < \lim_{t\to\infty} \rho_\psi(t)$

and ii) incorporate the desired performance specifications regarding the steady state error and the speed of convergence;

and design the desired velocities:

$$\begin{bmatrix} u_d \\ v_d \\ w_d \end{bmatrix} = \begin{bmatrix} \cos\psi & -\sin\psi & 0 \\ \sin\psi & \cos\psi & 0 \\ 0 & 0 & 1 \end{bmatrix}^{-1} \begin{bmatrix} -k_x \frac{e_x}{\rho_x(t)} \\ -k_y \frac{e_y}{\rho_y(t)} \\ -k_z \frac{e_z}{\rho_z(t)} \end{bmatrix} \quad (14)$$

$$r_d = -k_\psi \frac{e_\psi}{\rho_\psi(t)} \quad (15)$$

with positive control gains k_x, k_y, k_z, k_ψ.

II. Dynamic Controller

Select exponentially decreasing velocity performance functions $\rho_u(t)$, $\rho_v(t)$, $\rho_w(t)$, $\rho_r(t)$ that satisfy:

a. $\lvert u(0)-u_d(0)\rvert < \rho_u(0)$	$0<\rho_u(t)$	$0<\lim_{t\to\infty}\rho_u(t)$
b. $\lvert v(0)-v_d(0)\rvert < \rho_v(0)$	$0<\rho_v(t)$	$0<\lim_{t\to\infty}\rho_v(t)$
c. $\lvert w(0)-w_d(0)\rvert < \rho_w(0)$	$0<\rho_w(t)$	$0<\lim_{t\to\infty}\rho_w(t)$
d. $\lvert r(0)-r_d(0)\rvert < \rho_r(0)$	$0<\rho_r(t)$	$0<\lim_{t\to\infty}\rho_r(t)$

and design the external forces in the surge, sway and heave as well as the external torque around yaw as:

$$X=-k_u\frac{u-u_d}{\rho_u(t)},\ Y=-k_v\frac{u-u_d}{\rho_u(t)},\ Z=-k_w\frac{w-w_d}{\rho_w(t)},\ N=-k_r\frac{r-r_d}{\rho_r(t)} \quad (16)$$

with positive control gains k_u, k_v, k_w, k_r.

Remark 1: The proposed control scheme does not incorporate the vehicle's dynamic model parameters or knowledge of the external disturbances. Furthermore, no estimation (i.e., adaptive control) has been employed to acquire such knowledge. Moreover, compared with the traditional backstepping-like approaches, the proposed methodology proves significantly less complex. Notice that no hard calculations are required to output the proposed control signals thus making its implementation straightforward.

2) Stability Analysis: The main results of this work are summarized in the following theorem where it is proven that the aforementioned control scheme solves the tracking control problem presented at the beginning of this subsection.

Theorem 2: Consider: i) the underwater vehicle model (1)-(8), ii) the target described by $p_d=[x_d,y_d,z_d]^T$ and $n_d=\left[n_{x_d},n_{y_d},n_{z_d}\right]^T$ and the desired distance $\bar{d}$ from it at which hovering is required, iii) any initial configuration with the target lying inside the onboard camera's field of view, described by ψ_c and iv) the position/orientation errors defined in (11)-(13). There exist positive control gains k_x, k_y, k_z, k_ψ, k_u, k_v, k_w, k_r such that the proposed control scheme (14)-(16) guarantees that the vehicle approaches the hovering point $p_d-\bar{d}n_d$ with prescribed transient and steady state performance, keeping simultaneously the target in the camera's field on view, that is $\left|e_\psi(t)\right|<\psi_c$, $\forall t\geq 0$.

Proof: Let us first define the normalized errors:

$$\xi_x=\frac{e_x}{\rho_x(t)},\ \xi_x=\frac{e_y}{\rho_y(t)},\ \xi_z=\frac{e_z}{\rho_z(t)},\ \xi_\psi=\frac{e_\psi}{\rho_\psi(t)} \quad (17)$$

$$\xi_u=\frac{u-u_d}{\rho_u(t)},\ \xi_v=\frac{v-v_d}{\rho_v(t)},\ \xi_w=\frac{w-w_d}{\rho_w(t)},\ \xi_r=\frac{r-r_d}{\rho_r(t)} \quad (18)$$

and the overall closed loop system state vector as:

$$\xi=\left[\xi_x,\xi_y,\xi_z,\xi_\psi,\xi_u,\xi_v,\xi_w,\xi_r\right]^T.$$

Differentiating the normalized errors with respect to time and substituting (1)-(8) as well as (14)-(16), we obtain in a compact form, the dynamical system of the overall state vector:

$$\dot{\xi}=h(t,\xi) \quad (19)$$

where the function $h(t,\xi)$ includes all terms found at the right hand side after the differentiation of ξ. Let us also define the open set:

$$\Omega_\xi=\underbrace{(-1,1)\times\cdots\times(-1,1)}_{\text{8-times}}.$$

In the sequel, we proceed in two phases. First, the existence of a maximal solution $\xi(t)$ of (19) over the set Ω_ξ for a time interval $[0,\tau_{\max})$ (i.e., $\xi(t)\in\Omega_\xi$, $\forall t\in[0,\tau_{\max})$) is ensured. Then, we prove that the proposed control scheme guarantees, for all $t\in[0,\tau_{\max})$: a) the boundedness of all closed loop signals as well as that b) $\xi(t)$ remains strictly within a compact subset of Ω_ξ, which subsequently will lead by contradiction to $\tau_{\max}=\infty$ and consequently to the solution of the control problem stated at the beginning of Subsection III-B.

Phase A. The set Ω_ξ is nonempty and open. Moreover, owing to the selection of the performance functions $\rho_i(t)$ (i.e., $|e_i(0)|<\rho_i(0)$), $i\in\{x,y,z,\psi,u,v,w,r\}$ we conclude that $\xi(0)\in\Omega_\xi$. Additionally, due to the smoothness of a) the system nonlinearities and b) the proposed control scheme, over Ω_ξ, it can be easily verified that $h(t,\xi)$ is continuous on t and continuous for all $\xi\in\Omega_\xi$. Therefore, the hypotheses of Theorem 1 stated in Subsection II-D hold and the existence of a maximal solution $\xi(t)$ of (19) on a time interval $[0,\tau_{\max})$ such that $\xi(t)\in\Omega_\xi$, $\forall t\in[0,\tau_{\max})$ is ensured.

Phase B. We have proven in Phase A that $\xi(t)\in\Omega_\xi$, $\forall t\in[0,\tau_{\max})$ or equivalently that:

$$\xi_i(t)\in(-1,1),\ i\in\{x,y,z,\psi,u,v,w,r\} \quad (20)$$

for all $t\in[0,\tau_{\max})$. Therefore, the signals:

$$\varepsilon_i(t)=\ln\left(\frac{1+\xi_i(t)}{1-\xi_i(t)}\right),\ i\in\{x,y,z,\psi,u,v,w,r\} \quad (21)$$

are well defined for all $t\in[0,\tau_{\max})$. Consider now the positive definite and radially unbounded function $V_p=\frac{1}{2}\left(\varepsilon_x^2+\varepsilon_y^2+\varepsilon_z^2\right)$. Differentiating with respect to time, substituting (1)-(3) as well as employing (14),(15) and (18), we obtain:

$$\dot{V}_p=\left[\frac{\varepsilon_x}{\left(1-\xi_x^2\right)\rho_x(t)},\frac{\varepsilon_y}{\left(1-\xi_y^2\right)\rho_y(t)},\frac{\varepsilon_z}{\left(1-\xi_z^2\right)\rho_z(t)}\right] \times\left(\begin{bmatrix} -k_x\xi_x+\delta_x(t)-\xi_x\dot{\rho}_x(t)+\cos(\psi)\xi_u\rho_u(t)-\sin(\psi)\xi_v\rho_v(t) \\ -k_y\xi_y+\delta_y(t)-\xi_y\dot{\rho}_y(t)+\sin(\psi)\xi_u\rho_u(t)+\sin(\psi)\xi_v\rho_v(t) \\ -k_z\xi_z+\delta_z(t)-\xi_z\dot{\rho}_z(t)+\xi_w\rho_w(t) \end{bmatrix}\right).$$

Furthermore, utilizing (20) and the fact that $\dot{\rho}_x(t)$, $\dot{\rho}_y(t)$, $\dot{\rho}_z(t)$, $\rho_u(t)$, $\rho_v(t)$, $\rho_w(t)$, $\delta_x(t)$, $\delta_y(t)$, $\delta_z(t)$ are bounded by construction and by assumption, we arrive at:

$$\left|\delta_x(t)-\xi_x\dot{\rho}_x(t)+\cos(\psi)\xi_u\rho_u(t)-\sin(\psi)\xi_v\rho_v(t)\right|\leq\bar{F}_x$$
$$\left|\delta_y(t)-\xi_y\dot{\rho}_y(t)+\sin(\psi)\xi_u\rho_u(t)+\sin(\psi)\xi_v\rho_v(t)\right|\leq\bar{F}_y$$
$$\left|\delta_z(t)-\xi_z\dot{\rho}_z(t)+\xi_w\rho_w(t)\right|\leq\bar{F}_z$$

for some positive constants $\bar{F}_x$, $\bar{F}_y$, $\bar{F}_z$. Moreover, $\frac{1}{(1-\xi_x^2)}, \frac{1}{(1-\xi_y^2)}, \frac{1}{(1-\xi_z^2)} > 1$ and $\rho_x(t), \rho_y(t), \rho_z(t) > 0$. Therefore, employing the fact that ε_i and ξ_i have the same sign (see (21)), $i \in \{x,y,z,\psi,u,v,w,r\}$, we conclude that $\dot{V}_p$ is negative when the following inequalities hold: $|\xi_x(t)| > \frac{\bar{F}_x}{k_x}, |\xi_y(t)| > \frac{\bar{F}_y}{k_y}, |\xi_z(t)| > \frac{\bar{F}_z}{k_z}$. Thus, if we select k_x, k_y, k_z such that $\frac{\bar{F}_x}{k_x}, \frac{\bar{F}_y}{k_y}, \frac{\bar{F}_z}{k_z} < 1$ then it can be easily concluded that:

$$-1 < -\frac{\bar{F}_i}{k_i} \leq \xi_i(t) \leq \frac{\bar{F}_i}{k_i} < 1, \; i \in \{x,y,z\} \tag{22}$$

for all $t \in [0, \tau_{\max})$. Subsequently, following similar analysis with $V_o = \frac{1}{2}\varepsilon_\psi^2$, we arrive at:

$$-1 < -\frac{\bar{F}_\psi}{k_\psi} \leq \xi_\psi(t) \leq \frac{\bar{F}_\psi}{k_\psi} < 1 \tag{23}$$

for a positive constant $\bar{F}_\psi$ and a gain k_ψ satisfying $k_\psi > \bar{F}_\psi$. Additionally, the desired velocities u_d, v_d, w_d, r_d remain bounded for all $t \in [0, \tau_{\max})$. Thus, invoking (18), the boundedness of $u(t)$, $v(t)$, $w(t)$, $r(t)$ for all $t \in [0, \tau_{\max})$ is also deduced. Finally, differentiating (14) and (15) with respect to time and after some algebraic manipulations it is straightforward to obtain the boundedness of $\dot{u}_d(t)$, $\dot{v}_d(t)$, $\dot{w}_d(t)$, $\dot{r}_d(t)$, $\forall t \in [0, \tau_{\max})$.

Applying the aforementioned line of proof for the dynamic part of the vehicle (5)-(8), considering $V_d = \frac{1}{2}\left(\varepsilon_u^2 + \varepsilon_v^2 + \varepsilon_w^2 + \varepsilon_r^2\right)$ and the proposed control law (16), we arrive at:

$$-1 < -\frac{\bar{F}_i}{k_i} \leq \xi_i(t) \leq \frac{\bar{F}_i}{k_i} < 1 \tag{24}$$

for some positive constants $\bar{F}_i$ and control gains k_i satisfying $k_i > \bar{F}_i$, $i \in \{u,v,w,r\}$ as well as at the boundedness of the control law (16) for all $t \in [0, \tau_{\max})$.

Up to this point, what remains to be shown is that $\tau_{\max} = \infty$. Notice that (22), (23) and (24) imply that $\xi(t) \in \Omega_\xi^{'}$, $\forall t \in [0, \tau_{\max})$, where:

$$\Omega_\xi^{'} = \prod_{i \in \{x,y,z,\psi,u,v,w,r\}} \left[-\frac{\bar{F}_i}{k_i}, \frac{\bar{F}_i}{k_i}\right]$$

is a nonempty and compact set. Moreover, it can be easily verified that $\Omega_\xi^{'} \subset \Omega_\xi$ for $k_i > \bar{F}_i$, $i \in \{x,y,z,\psi,u,v,w,r\}$. Hence, assuming $\tau_{\max} < \infty$ and since $\Omega_\xi^{'} \subset \Omega_\xi$, Proposition 1 in Subsection II-D dictates the existence of a time instant $t^{'} \in [0, \tau_{\max})$ such that $\xi\left(t^{'}\right) \notin \Omega_\xi^{'}$, which is a clear contradiction. Therefore, $\tau_{\max} = \infty$. As a result, all closed loop signals remain bounded and moreover $\xi(t) \in \Omega_\xi^{'} \subset \Omega_\xi$, $\forall t \geq 0$. Additionally, from (17), (22) and (23), we conclude that:

$$-\rho_i(t) < -\frac{\bar{F}_i}{k_i}\rho_i(t) \leq e_i(t) \leq \frac{\bar{F}_i}{k_i}\rho_i(t) < \rho_i(t)$$

for $i \in \{x,y,z,\psi\}$, $\forall t \geq 0$ and consequently that prescribed performance is achieved, as presented in Subsection II-C. Finally, since the exponential decaying orientation performance function $\rho_\psi(t)$ was designed such that $\rho_\psi(0) < \psi_c$ then it follows that $\left|e_\psi(t)\right| < \rho_\psi(t) < \psi_c$ for all $t \geq 0$ (that is, the target lies in the camera's field of view for all $t \geq 0$), which completes the proof.

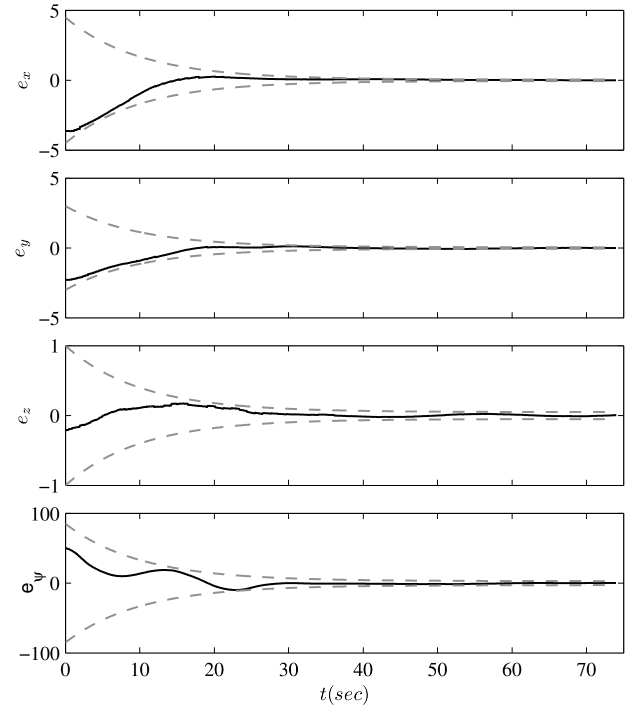

Fig. 1. Tracking error evolution. The grey dashed lines indicate the desired performance bounds. The black solid lines indicate the evolution of $e_x(t)$, $e_y(t)$, $e_z(t)$ and $e_\psi(t)$.

Remark 2: From the aforementioned proof, it is worth noticing that the proposed control scheme achieves its goals without residing to the need of rendering $\frac{\bar{F}_i}{k_i}$, $i \in \{x,y,z,\psi,u,v,w,r\}$ arbitrarily small, through extreme values of the control gains k_i, $i \in \{x,y,z,\psi,u,v,w,r\}$. In this respect, the actual tracking performance, which is determined by the performance functions $\rho_x(t)$, $\rho_y(t)$, $\rho_z(t)$, $\rho_\psi(t)$, becomes isolated against model uncertainties thus extending the robustness of the proposed control scheme.

Remark 3: Assuming that the target initially lies inside the onboard camera's field of view (i.e., $\left|e_\psi(0)\right| < \psi_c$), the proposed controller guarantees, through the appropriate selection of the exponentially decaying orientation performance function $\rho_\psi(t)$ (i.e., $\left|e_\psi(0)\right| < \rho_\psi(0) < \psi_c$), that the target never escapes the field of view. Thus, there is no need of employing special techniques (e.g., potential fields, navigation functions, planning, etc.) in the control loop to preserve the visual contact of the target, which is important in visual servo control schemes since the feedback depends mainly on the visual contact of the vehicle and the target.

IV. EXPERIMENTS

To illustrate the performance of the proposed visual servo control scheme, an experimental procedure was carried out. The experiments took place inside a water tank using the Girona500 AUV. A panel consisting of valves and handles located inside the pool was used as the visual target. The goal of this experiment is to illustrate the ability of the proposed control scheme to navigate and stabilize the vehicle in front of the panel, while retaining the panel always inside the the camera's field of view. The vehicle starts from an arbitrary initial configuration with the panel lying inside the onboard camera's field of view. The required transient and steady state specifications, (that is, maximum steady state position errors 0.05m, maximum steady state orientation error 5^o and exponential convergence $e^{-0.1t}$), are described by the following performance functions: $\rho_x(t) = (4.5-0.05)e^{-0.1t}+0.05$, $\rho_y(t) = (3.0-0.05)e^{-0.1t}+0.05$, $\rho_z(t) = (1-0.05)e^{-0.1t}+0.05$, $\rho_\psi(t) = (85-5)e^{-0.1t}+5$, $\rho_u(t) = (1-0.1)e^{-0.1t}+0.1$, $\rho_v(t) = (1-0.1)e^{-0.1t}+0.1$, $\rho_w(t) = (1-0.1)e^{-0.1t}+0.1$, $\rho_r(t) = (1-0.1)e^{-0.1t}+0.1$. Given that the angle of view of the onboard camera is $\psi_c = 90^o$, notice also that we have selected the orientation performance function $\rho_\psi(t)$ such that $\rho_\psi(0) = 85^o < \psi_c$ which guarantees that the target never escapes the camera's field of view. Finally, the control gains were chosen as follows: $k_x = 1$, $k_y = 0.5$, $k_z = 0.5$, $k_\psi = 0.5$, $k_u = 15$, $k_v = 7.5$, $k_w = 15$, $k_r = 7.5$.

The tracking error evolution is depicted in Fig. 1. The grey dashed lines indicate the desired performance bounds and the black solid lines indicate the evolution of the tracking errors $e_x(t)$, $e_y(t)$, $e_z(t)$ and $e_\psi(t)$ respectively. Notice that all errors have met the transient and steady state specifications imposed by the previously selected performance function. As it is demonstrated by the experiments and predicted from the theoretical analysis, the control objective has been achieved. However, it should be noted that we were not able to create external disturbances in the form of waves and currents with the existing setup, hence, future directions would involve experiments with real conditions in the open sea to verify the efficiency of the proposed scheme.

V. VIDEO

This paper is accompanied by a small video demonstrating the efficiency of the proposed visual servo control scheme, using the Girona500 AUV inside the CIRS water tank facilities at the University of Girona in Spain. The video presents the experimental procedure described in Section IV. It illustrates not only the tracking performance of the controller but also its ability to always retain the target inside the camera's field of view.

VI. CONCLUSIONS

This paper describes the design and implementation of a novel visual servo control scheme for an Autonomous Underwater Vehicle (AUV). The proposed control scheme does not utilize the vehicle's dynamic model parameters and guarantees prescribed transient and steady state performance despite the presence of external disturbances. The purpose of the controller is to navigate and stabilize the vehicle towards a visual target. The proposed scheme is of low complexity and guarantees the satisfaction of visual constraints, e.g., keeping the target inside the onboard camera's field of view. Finally, the resulting control scheme has analytically guaranteed stability and convergence properties, while its applicability and performance were experimentally verified using the Girona500 AUV.

REFERENCES

[1] J. Lots, D. Lane, E. Trucco, and F. Chaumette, "A 2d visual servoing for underwater vehicle station keeping," *Proc. of IEEE International Conference on Robotics and Automation*, pp. 2767–2772, 2001.

[2] C. Silpa-Anan, T. Brinsmead, S. Abdallah, and A. Zelinsky, "Preliminary experiments in visual servo control for autonomous underwater vehicle," *Proc. of IEEE/RSJ Intelligent Robots and Systems*, pp. 1824–1829, 2001.

[3] S. Negahdaripour and P. Firoozfam, "An rov stereovision system for ship-hull inspection," *IEEE Journal of Oceanic Engineering*, pp. 551–564, 2006.

[4] Y. Mezouar and F. Chaumette, "Path planning in image space for robust visual servoing," *Proc. of IEEE International Conference on Robotics and Automation*, pp. 2759–2764, 2000.

[5] B. Thuilot, P. Martinet, L. Cordesses, and J. Gallice, "Position based visual servoing: keeping the object in the field of vision," *Proc. of IEEE International Conference on Robotics and Automation*, pp. 1624 –1629, 2002.

[6] S. Bhattacharya, R. Murrieta, and S. Hutchinson, "Optimal paths for landmark-based navigation by differential-drive vehicles with field-of-view constraints," *IEEE Transactions on Robotics*, pp. 47–59, 2007.

[7] P. Murrieri, D. Fontanelli, and A. Bicchi, "A hybrid-control approach to the parking problem of a wheeled vehicle using limited view-angle visual feedback," *The International Journal of Robotics Research*, pp. 437–448, 2004.

[8] G. Karras and K. Kyriakopoulos, "Visual servo control of an underwater vehicle using a laser vision system," *Proc. of IEEE/RSJ Intelligent Robots and Systems*, pp. 4116–4122, 2008.

[9] G. Karras, S. Loizou, and K. Kyriakopoulos, "Towards semi-autonomous operation of under-actuated underwater vehicles: sensor fusion, on-line identification and visual servo control," *Autonomous Robots*, pp. 67–86, 2011.

[10] T. Fossen, "Guidance and control of ocean vehicles," *Wiley, New York*, 1994.

[11] C. P. Bechlioulis and G. A. Rovithakis, "Robust adaptive control of feedback linearizable mimo nonlinear systems with prescribed performance," *IEEE Transactions on Automatic Control*, vol. 53, no. 9, pp. 2090–2099, 2008.

[12] ——, "Adaptive control with guaranteed transient and steady state tracking error bounds for strict feedback systems," *Automatica*, vol. 45, no. 2, pp. 532–538, 2009.

[13] ——, "Prescribed performance adaptive control for multi-input multi-output affine in the control nonlinear systems," *IEEE Transactions on Automatic Control*, vol. 55, no. 5, pp. 1220–1226, 2010.

[14] E. D. Sontag, *Mathematical Control Theory*. London, U.K.: Springer, 1998.

[15] E. Rublee, V. Rabaud, K. Konolige, and G. Bradski, "Orb: An efficient alternative to sift or surf," in *Computer Vision (ICCV), 2011 IEEE International Conference on*, nov. 2011, pp. 2564–2571.

[16] E. Rosten and T. Drummond, "Machine learning for high-speed corner detection," in *In European Conference on Computer Vision*, 2006, pp. 430–443.

[17] M. Calonder, V. Lepetit, C. Strecha, and P. Fua, "Brief: binary robust independent elementary features," in *Proceedings of the 11th European conference on Computer vision: Part IV*, ser. ECCV'10. Berlin, Heidelberg: Springer-Verlag, 2010, pp. 778–792. [Online]. Available: http://dl.acm.org/citation.cfm?id=1888089.1888148

[18] D. G. Lowe, "Distinctive image features from scale-invariant keypoints," *Int. J. Comput. Vision*, vol. 60, no. 2, pp. 91–110, Nov. 2004. [Online]. Available: http://dx.doi.org/10.1023/B:VISI.0000029664.99615.94

[19] H. Bay, A. Ess, T. Tuytelaars, and L. Van Gool, "Speeded-up robust features (surf)," *Comput. Vis. Image Underst.*, vol. 110, no. 3, pp. 346–359, June 2008. [Online]. Available: http://dx.doi.org/10.1016/j.cviu.2007.09.014